94. Jose B, Taracad K V, Tanmaya J, Ute K, Craig M F, David R, Leone S, *Polyhedron*, **52**(2013)128.
95. Priya P N, Sandeep P N, Srinivatsa B, Vidyanand K R, *Eur J Med Chem*, **79**(2014) 47.
96. Safaa Eldin H E, Dina M A, Eman H A, Elham A A, *Spectrochimica acta A,* **79** (2011) 1331.
97. Ramsey A S, David F, Han X L, Bruce K C, Kristin M F, Lynne C, Joseph M T, Laurie A T, *J Inorg Biochem,* **137** (2014) 1.
98. Xia-Bing F, Gui-Tian W, Dan-Dan L, *J Photochem photobiol A: Chem*, **276** (2014) 83.
99. Guo-Wu L, Yue W, Qiao-Mei J, Tao-Tao Y, *Inorg Chim Acta*, **382** (2012) 35.
100. Rahman A, Mohd A, Farukh A, *Spectrochimica Acta A, Mol Biomol Spectrosc*, **131** (2014) 625.

Chapter-III

Quinoxaline Schiff base Complexes

3.1. Introduction

Quinoxaline, also called as benzopyrazine, in organic chemistry, is a heterocyclic compound containing a ring complex made up of a benzene ring and a pyrazine ring and they are isomeric with cinnolenes, phthalazines and quinazolines. There are a number of processes available to generate quinoxaline but generally, they are synthesized by the condensation of 1, 2-dicarbonyls with 1, 2-diamines in presence of suitable catalyst using various solvent systems. They have been widely used in dyes, pharmaceuticals[1,2] and quinoxaline ring moiety constitute part of the chemical structures of various antibiotics such as *Echinomycin, Carbodox, Aspergillic acid, Levomycin and Actinoleutin*[3] that are known to inhibit growth of gram positive bacteria and are active against various transplantable tumors. They possess well known biological activities including anti-tumor[4], anti-cancer[5,6], anti-amoebic[7], anti-viral[8], anti-convulsant[9], anti-malarial[10], anti-tuberculosis[11,12,] anti-bacterial and fungal[13,14], anti-histaminic[15], anti-plasmodial activity[16], anti-leishmanic agents[17], electroluminescent materials[18], anti-inflammatory[19,20], anti-trypanosomal activity[21], Ca uptake/ Release inhibitor[22] and inhibit vascular smooth muscle cell proliferation.

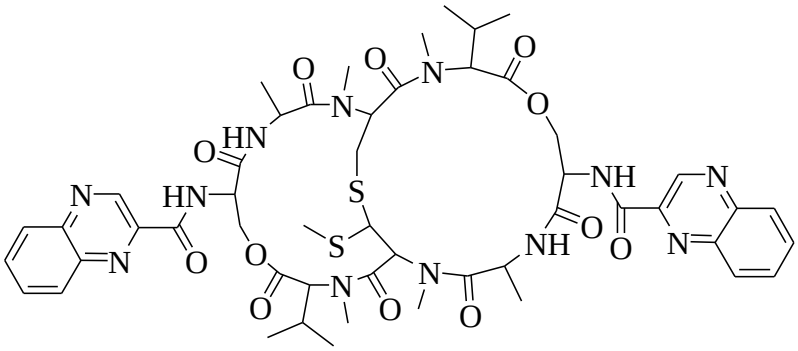

Echinomycin

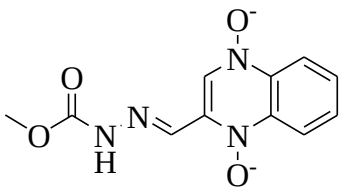

Carbodox

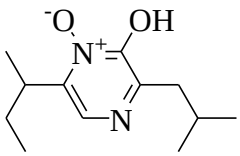

Aspergillic acid

The complexes of these bioactive quinoxalines are not found much in literature and the work described in this chapter describes the synthesis of the bioactive quinoxaline derivative and their metal complexes, their antimicrobial activity against several bacterial and fungal strains, their cytotoxicity, anti-oxidant properties and their DNA

interactions using absorption and emission measurements. The molecular structure of the quinoxaline Schiff base ligand and Cu(II) complex was investigated theoretically. The optimized molecular structure was obtained from Gaussian 09 program.

3. 2. Experimental Work

3. 2. 1. Synthesis of ligand

3. 2.1.1 Synthesis of 1,4-dihydroquinoxaline-2,3-dione (I)

A solution of oxalic acid dihydrate (0.238 mol, 30 g) in H_2O (100 mL) was heated to 100°C and concentrated HCl 4.5 mL was added, followed by *o*-phenylenediamine (0.204 mol, 22 g) with stirring, temperature was maintained at 100°C for 20 min. the mixture cooled by addition of ice. The precipitate obtained was filtered, washed with water and recrystallized from ethanol. Yield: 85%, m.pt: 160-162°C, Anal. Calcd (%) for $C_8H_6N_2O_2$: C, 59.26; H, 3.73; N, 17.28; found (%): C, 59.28; H, 3.70; N, 17.27. EI-MS: Found m/z=162.15(M+) calculated m/z=162.04 for M+. IR (KBr, cm^{-1}): 1718 γ(C=O), 3121 γ(-NH). ^{1}H-NMR (DMSO-d^6): δ 7.029-7.123(m, 4H, aromatic); δ 8.014(s, 1H, NH). ^{13}C-NMR (DMSO-d6): δ 155.95 (C=O); δ 115 – δ 126(aromatic).

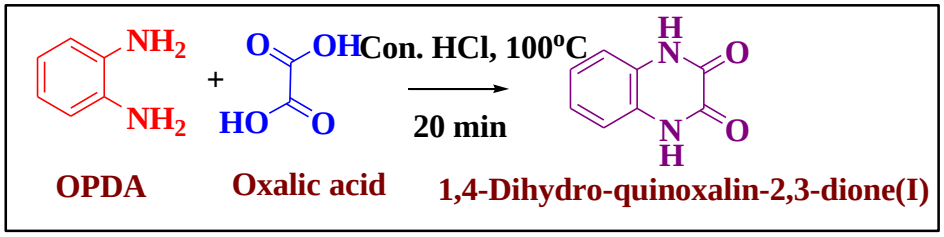

3.2.1.2. Synthesis of 3-[(2-aminoethyl) amino]quinoxalin-2(1H)-one(II)

A mixture of the quinoxalin-2,3-dione **(I)** (0.062 mol, 10.04 g), ethylene diamine (1 mole, 50 mL) and water (50 mL) was refluxed for 2 h, then cooled to room temperature, the precipitate was filtered, washed with water and crystallized from 2-butanol. Yield: 78%. m.pt: 181-183°C. Anal. calcd (%) for $C_{10}H_{12}N_4O$: C, 58.81; H, 5.92; N, 27.43; found(%): C, 58.79; H, 5.95; N, 27.39. EI-MS; Found m/z=204.23(M+) calculated m/z= 204.10 for M+. IR (KBr, cm^{-1}); 1718 γ(C=O); 3320, 3304 (-NH_2). ^{1}H-NMR: δ 6.798- δ 6.956(m, 4H, aromatic), δ 3.922(t, 2H, CH_2), δ 8.612(s, 1H, CONH), δ 3.400(m, 2H, CH_2), δ 2.425(1H, t, NH), δ 2.425 (2H, t, NH_2). ^{13}C-NMR: δ 115-123(aromatic), δ 48.7(CH_2), δ 49.7(CH_2), 157.8 (C=N), 163.0 (C=O).

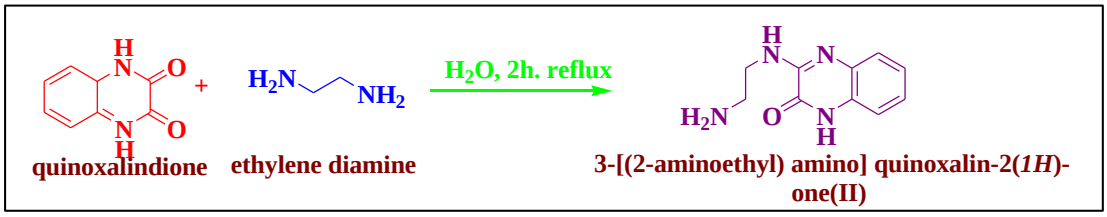

3.2.1.3. Synthesis of 3-[(2-{[(E)-(hydroxyphenyl) methylidene]amino} ethyl) amino] quinoxalin-2(1H)-one(III) (L)

An equimolar amount of 3-[(2-aminoethyl) amino] quinoxalin-2(1*H*)-one **(II)** and salicylaldehyde in ethanol (20 mL) was refluxed for 5h. Upon cooling, the precipitate obtained, was filtered, dried and crystallized from ethanol [23]. Yield: 64%. M. P: 203-205°C. Anal. calcd (%) for $C_{17}H_{16}N_4O_2$: C, 66.19; H, 5.23; N, 18.86. Found(%): C, 66.12; H, 5.38; N, 18. 75. EI-MS; Found m/z=308.16(M+) calculated m/z= 308.06 for M+.). IR (KBr, cm^{-1}): 1666 γ(C=O), 1620 γ(C=N, free), 1530 γ(C=N, ring), 1383 γ(C-O phenolic). ^{1}H-NMR: δ 6.850- δ6.901 (m, 4H, aromatic), δ 3.922(t, 2H, CH_2), δ 8.11(s, 1H, -CH=N), δ 5.023(s, 1H, OH), δ 2.435(t, 2H, CH_2), . δ 8.11(s, 1H,NH). ^{13}C-NMR:115-140 (aromatic), δ48.7(CH_2), δ49.7(CH_2), 157.8(C=N), 163.7(C=O).

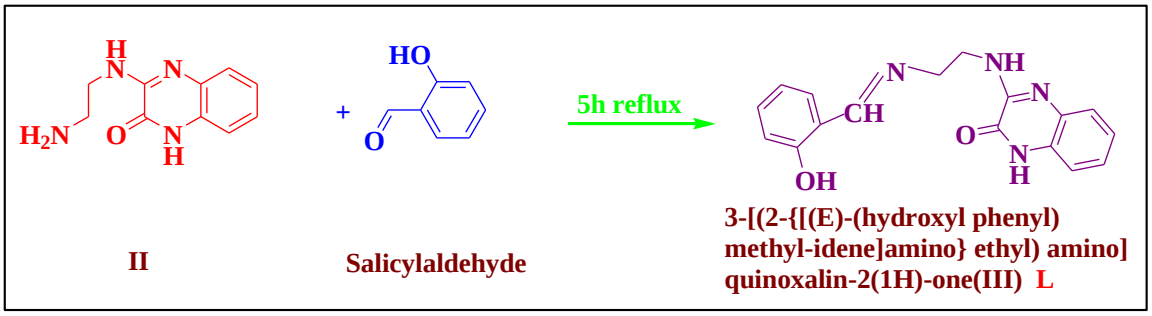

3.2.2. Synthesis of the complexes

An ethanolic solution of the metal chloride/nitrate(0.1M in 20mL ethanol) ($CrCl_3.3H_2O$/$FeCl_3.3H_2O$/$MnCl_2.3H_2O$/$CuCl_2.3H_2O$/$CoCl_2.6H_2O$/$Ni(NO_3)_2$) was added to an ethanolic solution of quinoxaline Schiff base ligand **L** (0.2M in 20mL ethanol). The resulting mixture was refluxed for 5h. After completion, the reaction mixture was filtered, washed with ether, dried and recrystallised from ethanol.

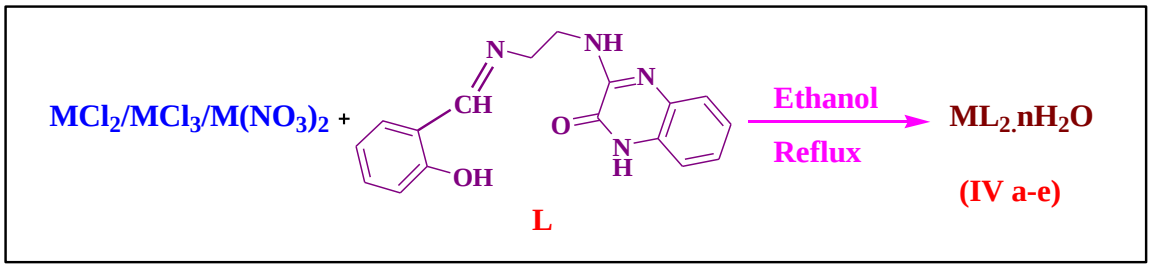

M = Cr(III), Fe(III), Co(II), Cu(II), Mn(II)

3.3. Characterisation of the ligand and the metal complexes

The synthesized ligand and the metal complexes were characterized by various spectral techniques *viz.*, FT-IR, UV-visible, ^{1}H and ^{13}C NMR, ESR, TGA spectral studies and using quantum mechanical calculations.

3.3.1. Instrumentation

Microanalytical data of the compounds were recorded in the *ElementarVario EL III* CHN Analyser. Metal estimations were determined complexometrically by standard EDTA titration. The FT-IR spectra of the samples were recorded on a *Shimadzu* spectrophotometer in 4000-400 cm^{-1}. ^{1}H and ^{13}C NMR spectra were recorded on a *Jeol* 400 MHz Spectrometer with TMS as an internal standard. The UV-visible spectra were recorded on an *Elico SL 159* UV-Vis Spectrophotometer. Magnetic susceptibility measurements of the complexes were carried out by *Guoy balance* using copper sulphate as the calibrant. The magnetic susceptibility of the metal complexes were calculated using the relation $\mu_{eff}=2.828(\chi_m.T)^{1/2}$ BM where χ_m is the molar susceptibility corrected using Pascal's constants for diamagnetism of all atoms in the compounds. The molar conductances of the complexes were measured using a S*ystronics* conductivity bridge at room temperature in DMSO solution. The thermal behavior of the complexes was studied using *Perkin Elmer STA 6000* thermoanalyser. EPR spectrum of Cu(II) complex was recorded at room temperature on an *ESR-JEOL-12* spectrometer using the DPPH as the g-marker. Energy Dispersive X-ray Detection (EDX) were taken in *Joel JSM*-6390 equipment, with an accelerating voltage of 20 KV. The molecular structure of the ligand in the ground state was optimized by UB3LYP methods with 6-31G (d) basis set. The antimicrobial activities of the ligand and its complexes were carried out by disc diffusion method. The anti-cancer activity of the ligand and its complexes were carried out against

MCF-7 using MTT assay and was found to be good. The antioxidant activity of the complexes were found using DPPH radical scavenging assay.

3.3.2. Magnetic moment studies

The magnetic moment of the complexes has been calculated by determining the magnetic susceptibility using Gouy balance at room temperature. Copper sulphate was used as calibrant.

3.3.2.1. Procedure

A pyrex glass of uniform base of 1.5 cm and length 8 cm was used as a sample tube. The complex was taken in the sample tube. The sample tube was suspended from the hook of the Gouy balance and the height was adjusted so that the sample is in the middle of the pole pieces of the electro magnet. It was thus at the position of maximum field intensity.

When a magnetic field is applied (by switching on the current) the sample might be attracted towards the magnetic field, if it is paramagnetic. Therefore weights have to be added to the other pan to restore balance. The sample might be repelled by the magnetic field if it is diamagnetic. In this case weights have to be removed from the other pan. The weights added or subtracted was thus found out. The field strength (H) of the electromagnet was varied and the weight was found out each time. The susceptibility was calculated using the equation,

$$\chi_m = [2g/A]\ [m/H^2] = [2X980/3.14X0.035^2]\ [M/H^2]$$

On the other hand plot of m/H^2 can be made and susceptibility can be calculated from the slope of the straight line obtained.

$$\chi_m = 5.1 \times 10^5 \text{ (slope) erg} \quad \text{where slope} = m/H^2$$

The effective magnetic moment can be calculated from the susceptibility.

$$\mu_{eff} = 2.828\sqrt{\chi_m}.T$$

3.3.3. Computational procedures

All the calculations were performed by using Gaussian 09 package and Gauss-View molecular visualization programs on the personal computer without restricting any symmetry for the ligand. The molecular structure of the ligand in the ground state (*in vacuo*) is optimized by UB3LYP methods with 6-31G (d) basis set. Besides, the nonlinear optical effects, the molecular electrostatic potential (MEP), frontier molecular orbitals (FMO), and the Mulliken population analysis of the ligand were determined by theoretical calculation results.

3.4. Pharmacology

3.4.1. Antimicrobial activity

The antibacterial activity of the ligand and the metal complexes were screened for gram positive bacteria and gram negative bacteria namely *Bacillus subtilis*, *Staphylococcus aureus*, *Klebsiella pneumonia*, *Salmonella paratyphi* by the disc diffusion method using agar nutrient as the medium. The antifungal activities were screened for the organisms *Aspergillus niger*, *Candida albicans* by the disc diffusion method cultured on potato dextrose agar as medium. The plate was incubated 24h for bacteria and 72h for fungi. During this period, the test solution diffused and the growth of the inoculated microorganisms was affected. The inhibition zone was developed, at which the concentration was noted.

The given test samples were dissolved in distilled water (5mg/mL) for assessing their antibacterial activity by well diffusion method. All the microbial cultures were analyzed for their susceptibility / resistance pattern to test samples by well diffusion method using Mueller Hinton agar medium for bacteria and Sabrose Dextrose Agar medium for fungus. Sterile medium was dispensed into sterile petri dishes aseptically. Enriched broth cultures (24h for bacteria and 48h for fungus, incubated) were used as inoculum. Using sterile cotton swab, the test organisms were swabbed over the surface of the agar plate aseptically. In each of these plates, wells (10 mm) were cut out using sterile cork borer. The samples were dissolved in DMSO and different concentration (20-80 µg/ml) of the sample was loaded onto the wells. The plates were incubated at 37^{o}C (for 24h for bacteria and 96 h for fungus) in upright position. Solvent was used as control. After the incubation, the diameter of the inhibition zones was observed[24].

3.4.2. In-vitro anticancer activity-Cell treatment procedure and MTT assay

The monolayer cells were detached with trypsin-ethylenediaminetetraacetic acid (EDTA) to make single cell suspensions and viable cells were counted using a hemocytometer and diluted with medium containing 5% FBS to give final density of 1×10^{5} cells/mL. Cell suspensions were seeded into 96-well plates at plating density of 10,000 cells/well and incubated to allow for cell attachment at 37°C. After 24 h, the cells were treated with serial concentrations of the test samples. They were initially dissolved in DMSO and diluted to twice the desired final maximum test concentration with serum free medium. Additional four, 2 fold serial dilutions were made to provide

a total of five sample concentrations. Aliquots of 100 µL of these different sample dilutions were added to the appropriate wells already containing 100µL of medium which resulted in the required final sample concentrations. Following drug addition, the plates were incubated for an additional 48 h at 37°C. The medium without samples served as control and triplicate was maintained for all concentrations. 3-[4,5-dimethylthiazol-2-yl]2,5-diphenyltetrazolium bromide (MTT) is a yellow water soluble tetrazolium salt. A mitochondrial enzyme in living cells, succinate-dehydrogenase, cleaves the tetrazolium ring, converting the MTT to an insoluble purple formazan. Therefore, the amount of formazan produced is directly proportional to the number of viable cells. After 48 h of incubation, 15 µL of MTT (5 mg/mL) in phosphate buffered saline (PBS) was added to each well and incubated at 37°C for 4 h. The medium with MTT was then flicked off and the formed formazan crystals were solubilized in 100 µL of DMSO and then measured the absorbance at 570 nm using micro plate reader. The % cell inhibition was determined using the formula,

$$\% \text{ cell Inhibition} = 100 - \text{Abs (sample)}/\text{Abs (control)} \times 100.$$

Nonlinear regression graph was plotted between % cell inhibition and $\log_{10}$ (concentration) and IC_{50} was determined using graph pad prism software[25].

3.4.3. DNA Binding

A solution of CT-DNA in 0.5mM NaCl/5mM Tris-HCl(pH 7.0) gave a ratio of UV absorbance at 260 and 280 nm(A_{260}/A_{280}) of 1.8-1.9, indicating that the DNA was sufficiently free of proteins. A concentrated stock solution of DNA was prepared in 5mM tris-HCl/50 mM NaCl in water at pH 7.0 and the concentration of CT-DNA was determined per nucleotide by taking the absorption coefficient (6600 $dm^3mol^{-1}cm^{-1}$) at 260 nm. Stock solutions were stored at 4°C and were used only for a maximum of 4 days. Doubly distilled water was used to prepare buffer solutions. Absorption titrations were performed by keeping the concentration of the complex constant (10 µM) and by varying the concentration of CT-DNA from 0 to 60 µM. The binding constant (K_b) for the complexes have been determined from the following equation.

$$\frac{[DNA]}{(\epsilon_A - \epsilon_F)} = \frac{[DNA]}{(\epsilon_B - \epsilon_F)} + \frac{1}{K_b(\epsilon_B - \epsilon_F)}$$

where ε_A, ε_B and ε_F correspond to the apparent, bound and free metal complex extinction coefficients respectively. A plot of [DNA] / (ε_A-ε_F) versus [DNA] gave a slope of $1/(\varepsilon_B-\varepsilon_F)$ and a Y intercept equal to $1/K_b(\varepsilon_B-\varepsilon_F)$, where K_b is the ratio of slope to the intercept[26,27].

One milliliter of 5mM TrisHCl buffer was transferred into the microtubes. Aliquots of complex and CT-DNA from their stock solution were added and made up to the required concentration by diluting with double distilled water. The solution was shaken well after all the additives were added and the measurements of absorption and emission were made against the appropriate blank solution. Absorption measurements were with a UV-visible spectrophotometer (*V-630, Jasco, UK*) using a 1-cm path length cell. Emission spectra were recorded on a spectrofluorimeter *(Jasco FP 750, UK)* equipped with a 150-W Xenon lamp.

3.4.4. Antioxidant activity

The 2, 2-diphenyl-2-picryl-hydrazyl (DPPH) radical scavenging activity of the compounds was measured according to the method of Elizabeth. The DPPH radical is a stable free radical having a λ_{max} at 517nm. A fixed concentration of the experimental compound (100µL) was added to a solution of DPPH in methanol (0.3mM, 1mL) and the final volume was made up to 4mL with double distilled water. DPPH solution with methanol was used as a positive control and methanol alone acted as a blank. The solution was incubated at 37°C for 30 min in dark. The decrease in absorbance of DPPH was measured at 517nm. The tests were run in triplicate, and various concentrations (20-100µg/mL) of the compounds showed 50% of activity. In addition, the percentage of activity was calculated using the formula, % of suppression ratio= $[(A_o-A_c)/A_o]\times100$. A_o and A_c are the absorbance in the absence and presence of the tested compounds respectively. The 50% activity (IC_{50}) can be calculated using the percentage of activity[28].

3.5. Results and discussion

A great deal of work has been reported on the synthesis and characterization of different Schiff bases. Due to the excellent donor properties of the azo group, these compounds are significant in the field of co-ordination chemistry. In addition to their additional ligational properties, Schiff bases and their complexes have important biological and industrial applications. In view of the above, an attempt was made to synthesize Schiff base complexes of Fe(III), Co(II), Mn(II), Cr(III), Cu(II), Ni(II) transition metals. The synthetic route of the ligand and the complexes are presented in Scheme 1 and 2 respectively.

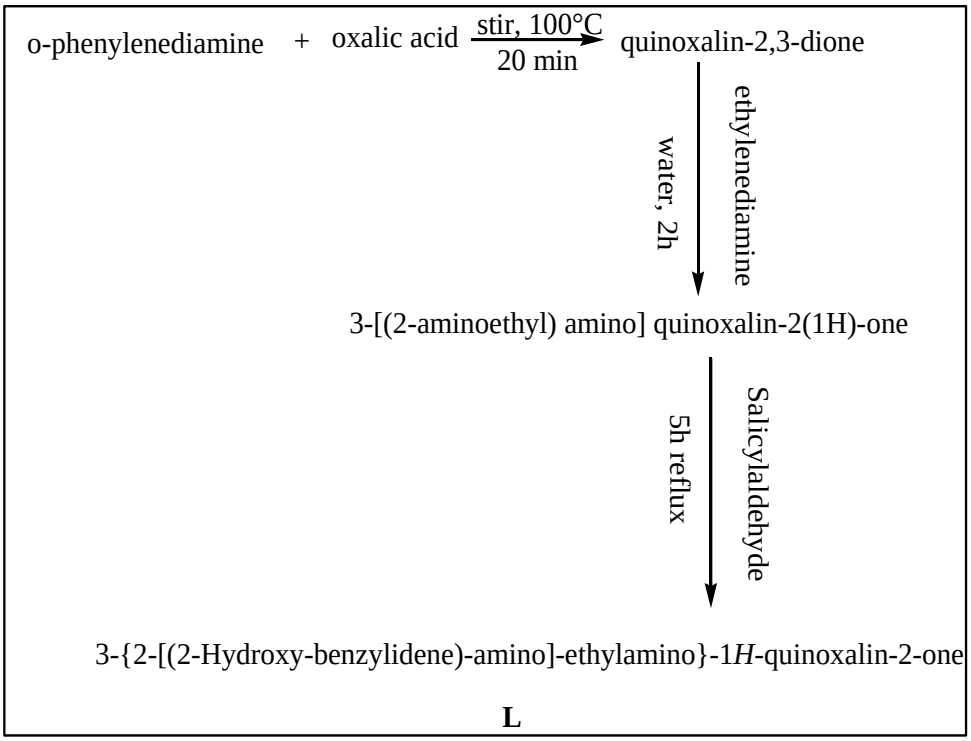

Scheme 1: Synthesis of Schiff base ligand

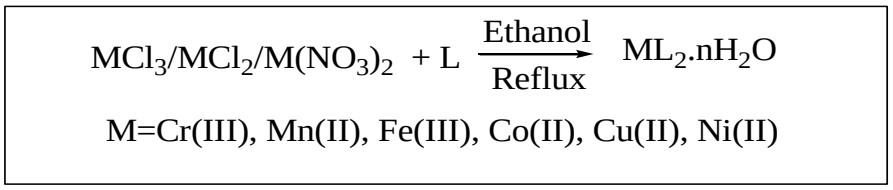

Scheme 2: Synthesis of the complexes

3.5.1. Analytical data

The quinoxaline Schiff base ligand and its complexes were synthesized and characterized using various spectral techniques. They are air stable for making all the physical measurements. The complexes are partially soluble in solvents like ethanol, methanol but freely soluble in DMF and DMSO and insoluble in water. The analytical data of the ligand and the complexes are in good agreement with the experimental values showing that the complexes are in 1:2 metal-ligand stoichiometry of the type ML_2 where in L acts as a bidentate OO donor and are shown in Table 3.1. The molar conductivities of 10^{-2} M of their solution at room temperature were measured. The negligible molar conductance of the complexes proves that the complexes are non-electrolytic in nature.

3. 5. 2. IR Spectral data of the ligand and complexes

The IR spectral data of the ligand shows a broad band around 2900 to 3300 cm^{-1} characteristic of phenolic –OH and the –NH group present in the Schiff base. The stretching frequencies at 1666, 1620, 1530 and 1383 cm^{-1} correspond to γ(C=O), γ(C=N), γ(C=N) (ring) and γ(C-O) present in the ligand respectively. All the complexes show changes (22 to 26cm^{-1}) in the stretching frequency of γ(C=O) confirming co-ordination of the ligand to the metal through carbonyl oxygen. The bands observed at the region 2900-3300cm^{-1} in Cr(III), Mn(II), Co(II) and Fe(III) complexes indicates the presence of water molecule. From IR data, it is clear that the metal is bonded through γ(-OH) after deprotonation. As the complexes are isolated in neutral media, the deprotonation of phenolic group is unavoidable. No band is observed at 3050cm^{-1} in nickel(II) complexes, suggesting the cleavage of intramolecularly hydrogen bonded –OH with subsequent deprotonation and co-ordination through phenolic oxygen. The multi-structured broad band at 3600-2600 cm^{-1} in Cr(III), Mn(II), Fe(III) and Co(II) complexes was attributed to γ(N-H), γ(C-H) ring and γ(O-H) (of co-ordinated water) and the appearance of band at 960-950 cm^{-1} confirmed the presence of co-ordinated water in Cr(III), Mn(II), Fe(III) and Co(III) complexes. New bands in the far IR are attributed to γ(M-O) and γ(M-N) in all complexes[29,30]. The IR stretching frequency of free γ(C=N) and γ(C=N) ring of the ligand is at 1620 and 1530 cm^{-1} respectively. There is no considerable shift in the stretching frequency of these bands in the complexes showing that these groups are not involved in co-ordination which is more obvious in the optimized geometry of the complex discussed later. The FT-IR stretching bands of the ligand and the complexes are given in Table 3.2 and the FT-IR spectra of the ligand and the complexes are given in Figs. 3.1a to 3.1g.

3. 5. 3. NMR Spectra

The NMR spectrum of the ligand were recorded in DMSO-d^6 solution and the ^1H and ^{13}C spectra of the ligand are shown in Figs. 3.2a to 3.2f for three stages respectively. The ^1H-NMR shows two multiplets around δ 6.850 to δ 6.901 ppm and δ 7.296 to δ 7.431ppm corresponding to the aromatic protons. A singlet at δ 8.612 and δ 8.11ppm corresponds to amide NH and azomethine proton respectively. The hydroxyl protons appear as singlet at δ 5.023 ppm. The peak for -CH_2 appears as triplet at δ 2.43 and δ 3.92 ppm. ^{13}C-NMR spectrum of the ligand shows thirteen singlets corresponding to various different carbons at their respective region.

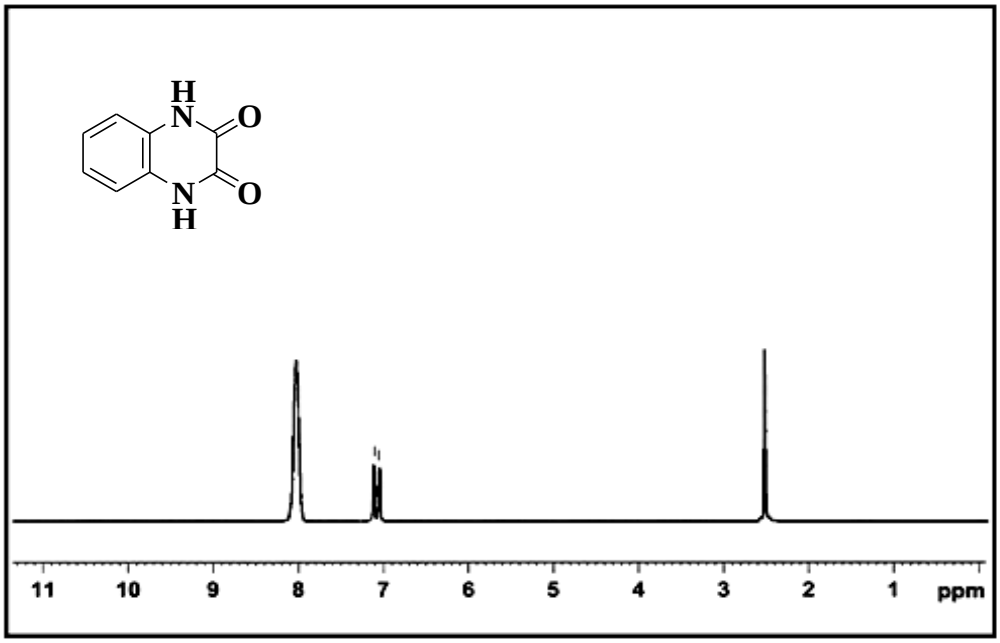

Fig. 3.2a. ^{1}H-NMR Spectrum of I

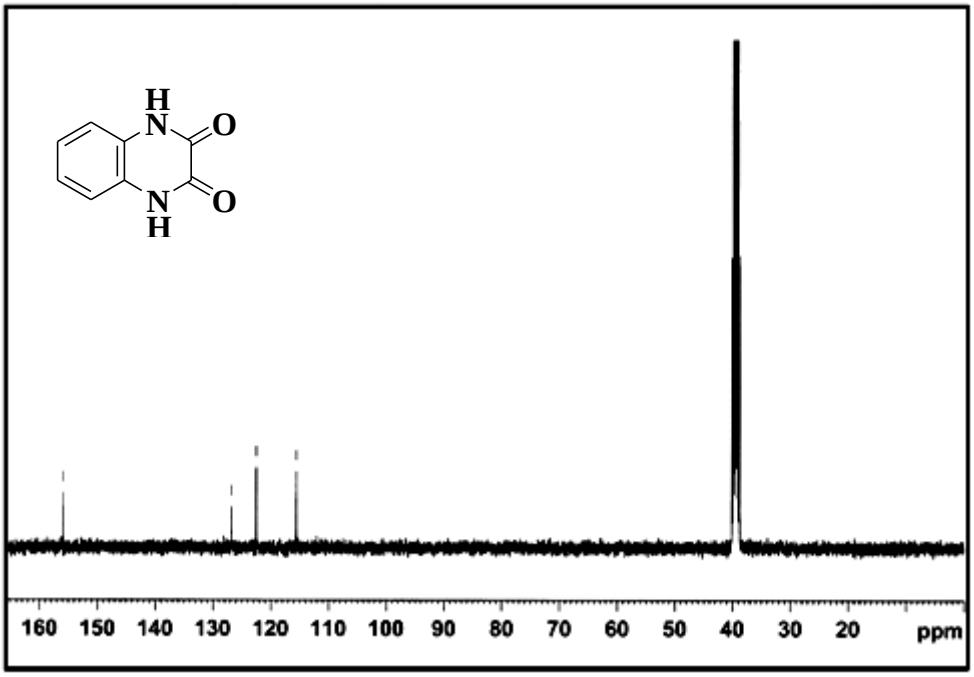

Fig. 3.2b. ^{13}C-NMR Spectrum of I

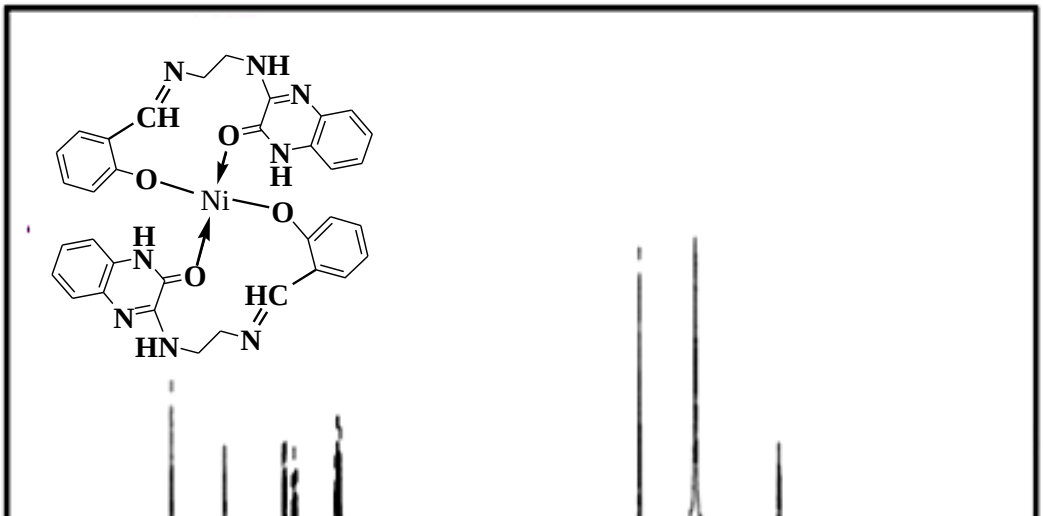

Fig. 3. 3. ^{1}H-NMR Spectrum of Ni(II) complex

The NMR spectrum of the Ni(II)complex shows the disappearance of –OH peak at δ 5.023 ppm proving the formation of the complex through phenolic –OH in the ligand. There is no de-shielding effect seen in –CH=N proving the non-involvement of the azomethine proton in the formation of the complex. The NMR spectrum of the complex is shown in Fig. 3.3.

3. 5. 4. Magnetic moment and electronic spectral data of the complexes

Magnetic moments and electronic spectral data are given in Table 3.3. The magnetic moments are in good agreement with the presence of unpaired electrons expected. The electronic spectrum of the ligand (Fig. 3.4a) shows two transitions at 320 and 360 nm which corresponds to π-π* and n-π* transitions.

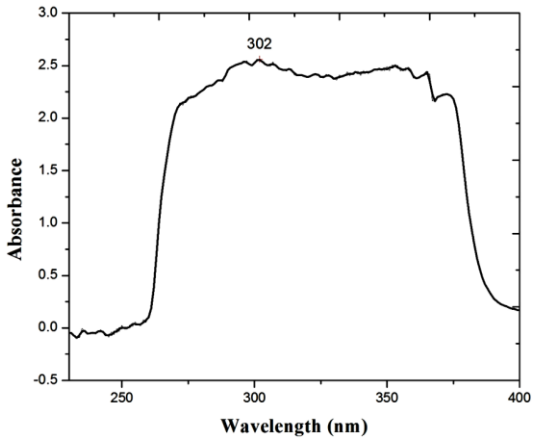

Fig. 3.4a. Electronic spectrum of the ligand

Generally in the spectra of all the metal complexes, the absorption bands due to π-π* and n-π* transitions that are observed in the free ligand lower than 400nm have shifted to higher wavelength due to the co-ordination of the ligand with the metal.

The electronic spectrum of the chromium complex (Fig. 3.4b) may be interpreted on the basis of an octahedral environment around chromium(III). The

complex showed three bands around 730, 420and 292nm which corresponds to $^4A_{2g} \rightarrow {}^4T_{2g}(F)$, $^4A_{2g} \rightarrow {}^4T_{2g}(F)$ and $^4A_{2g} \rightarrow {}^4T_{1g}(P)$ transitions respectively in the order of increasing energy. The observed room temperature magnetic moment value for this complex is around 4.15BM, consistent with the theoretical spin only value (μ_{eff}= 3.87BM) for Cr^{3+} system. Various ligand field parameters have been evaluated for the Cr(III) complex[31]. The value of the first spin allowed transition at 13698cm^{-1} is directly taken as 10Dq.

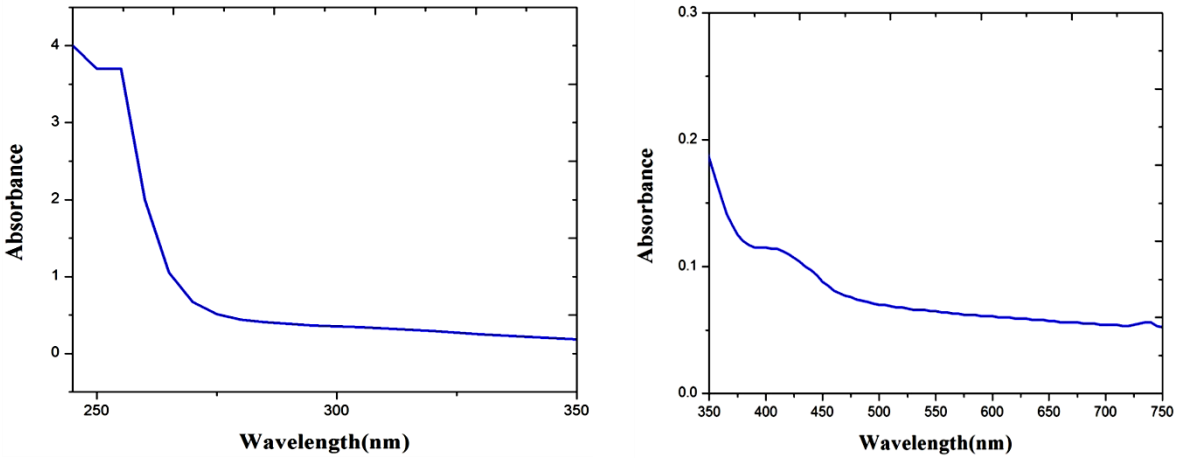

Fig. 3. 4b. Electronic spectrum of Cr(III) complex

The value of Racah parameter (B) can be calculated by the equation of Underhill and Billing B= ($\upsilon_3+\upsilon_2$-30Dq)/15. The observed value (732$\mp$ 100cm^{-1}) of the Racah electron repulsion parameter (B) was compared against the value (1030cm^{-1}) for the free Cr^{3+} ion, which indicates considerable covalent character of the metal-ligand bonds in this complex.

The electronic spectrum of the Mn(II) complex (Fig. 3.5) contains two bands at 447 and 328nm assignable $^6A_{1g} \rightarrow {}^4T_{2g}(G)$ and $^6A_{1g} \rightarrow {}^4E_{1g}$ respectively. Electronic transitions along with the magnetic moment value of 6.01 BM which is almost close to spin only value (6.01 BM) suggest high spin octahedral geometry for Mn(II) complex[32].

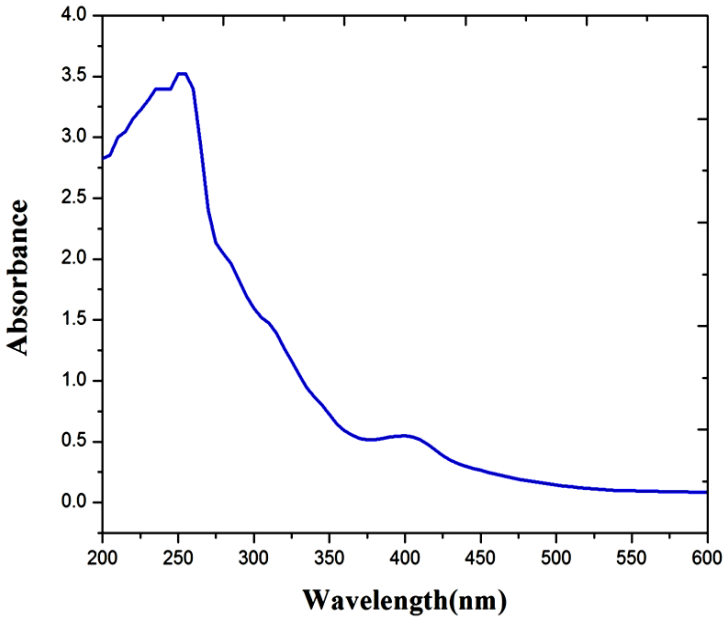

Fig. 3. 5. Electronic spectrum of Mn(II) complex

The electronic spectrum of the Fe(III) complex (Fig. 3.6) showed three weak bands at 530, 343 and 253nm which may be assigned to the transitions $^{6}A_{1g} \rightarrow {}^{4}T_{1g}(D)$, $^{6}A_{1g} \rightarrow {}^{4}T_{1g}$ and charge transfer respectively. Based on the electronic transitions together with magnetic moment value of 5.81BM, a high spin octahedral geometry has been proposed for Fe(III) complex[33].

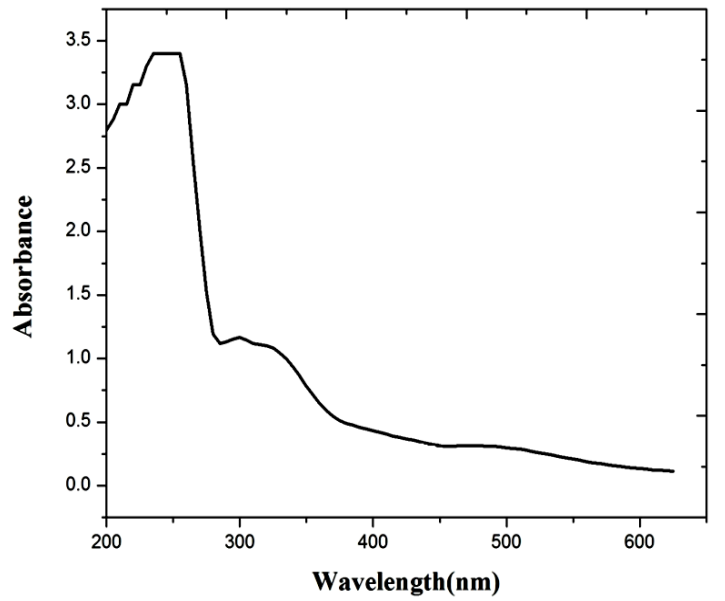

Fig. 3. 6. Electronic spectrum of Fe(III) complex

In general, octahedral, tetrahedral and square planar Co(II) complexes show magnetic moment between 4.7-5.2, 4.2-4.8 and 2.2 -2.9 BM respectively. The magnetic moment of the synthesized Co(II) complex is 4.71 confirming an octahedral geometry. The electronic spectrum of the complex (Fig. 3.7) showed two d-d transitions at 660 nm and 540 nm which corresponds to $^4T_{1g} \rightarrow {}^4A_{2g}(P)$ and $^4T_{1g} \rightarrow {}^4A_{2g}(F)$ transitions respectively. This indicates an octahedral configuration around Co(II) ions[34].

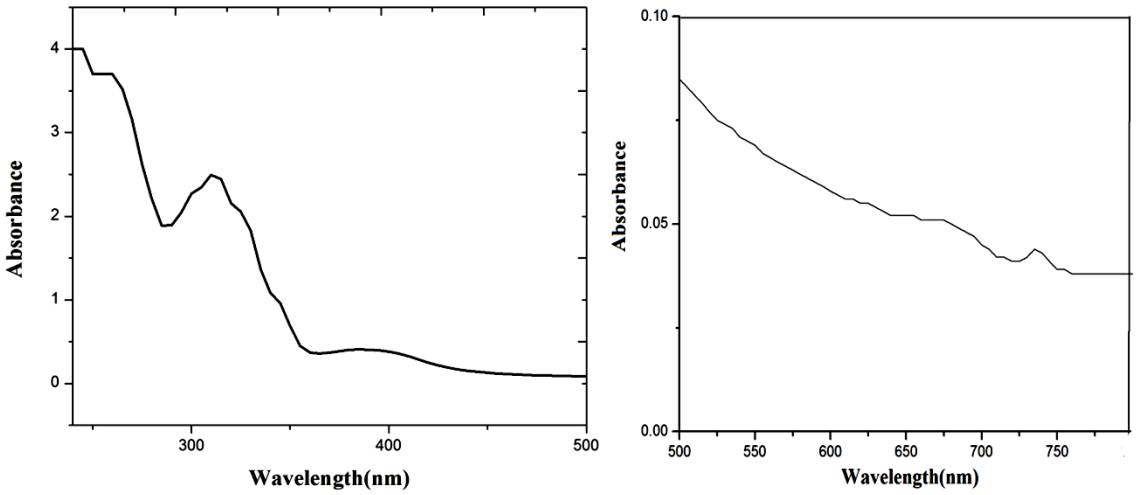

Fig. 3. 7. Electronic spectrum of Co(II) complex

The electronic spectrum of Ni(II) complex (Fig. 3.8) consists of two bands at about 553 and 410 nm assignable to $^1A_{1g} \rightarrow {}^1T_{2g}$ and charge transfer transitions respectively. Observed electronic transitions, the diamagnetic nature and red color of the complex suggests square planar geometry for Ni(II) complex[35].

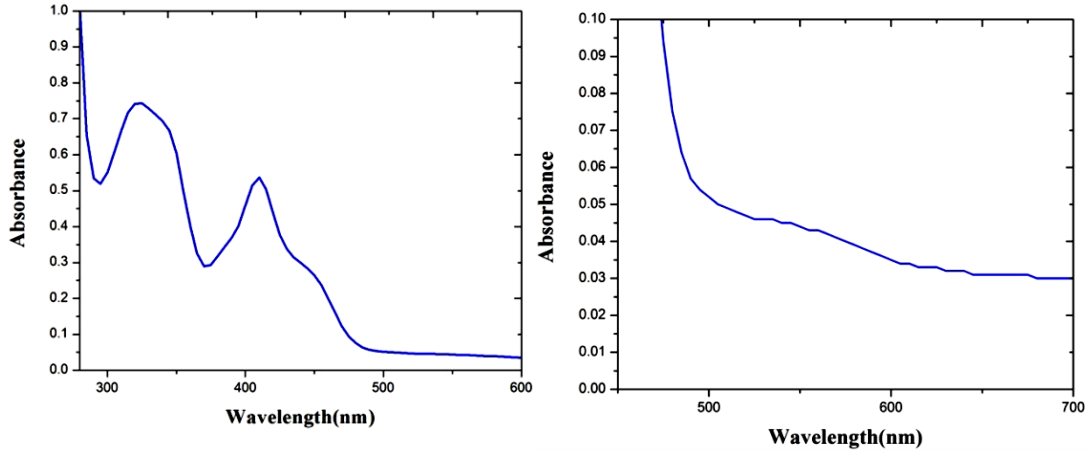

Fig. 3. 8. Electronic spectrum of Ni(II) complex

Cu(II) systems with square planar or close to square planar will have no absorption below 10000cm^{-1}. The transition at 406 nm is assigned as $^2B_{1g} \rightarrow {}^2A_{1g}$

transition and it is interpreted as square planar geometry. The broadness of the band can be taken as an indication of distortion from perfect planar symmetry. The absence of a band below 10000 cm^{-1} eliminates the possibility of a tetrahedral or pseudo-tetrahedral environment in these complexes[36, 37]. The square planar geometry of the Cu(II) complex (Fig. 3.9) is further confirmed by the measured magnetic moment value 1.87BM.

Table 3.3. Electronic spectral data of the Schiff base ligand and its complexes

Complex	**μ_{eff} (B.M)**	**υ_{max} (cm^{-1})**	**Assignments**
$C_{17}H_{16}N_4O_2$	-	360 320	n-π*, π-π*
$Cr(C_{17}H_{15}N_4O_2)_2(OH_2)Cl$	4.15	310 420 730	$^4A_{2g}\rightarrow{}^4T_{1g}(P)$ $^4A_{2g}\rightarrow{}^4T_{1g}(F)$ $^4A_{2g}\rightarrow{}^4T_{2g}(F)$
$Mn(C_{17}H_{15}N_4O_2)_2(OH_2)_2$	6.05	430 328	$^6A_{1g}\rightarrow{}^4T_{2g}(G)$ Charge transfer
$Fe(C_{17}H_{15}N_4O_2)_2(OH_2)Cl$	5.81	530 343 253	$^6A_{1g}\rightarrow{}^4T_{1g}(D)$ $^6A_{1g}\rightarrow{}^4T_{1g}$ Charge transfer
$Co(C_{17}H_{15}N_4O_2)_2(H_2O)_2$	4.71	540 660 730	$^4T_{1g}\rightarrow{}^4A_{2g}(P)$ $^4T_{1g}\rightarrow{}^4A_{2g}(F)$
$[Ni(C_{17}H_{15}N_4O_2)_2]$	0.0	410 553	Charge transfer $^1A_{1g}\rightarrow{}^1T_{2g}$
$[Cu(C_{17}H_{15}N_4O_2)_2].\ H_2O$	1.87	390 560 600	$^4B_{2g}\rightarrow{}^2A_{1g}$ $^4B_{2g}\rightarrow{}^2B_{1g}$ $^4B_{2g}\rightarrow{}^2E_g$

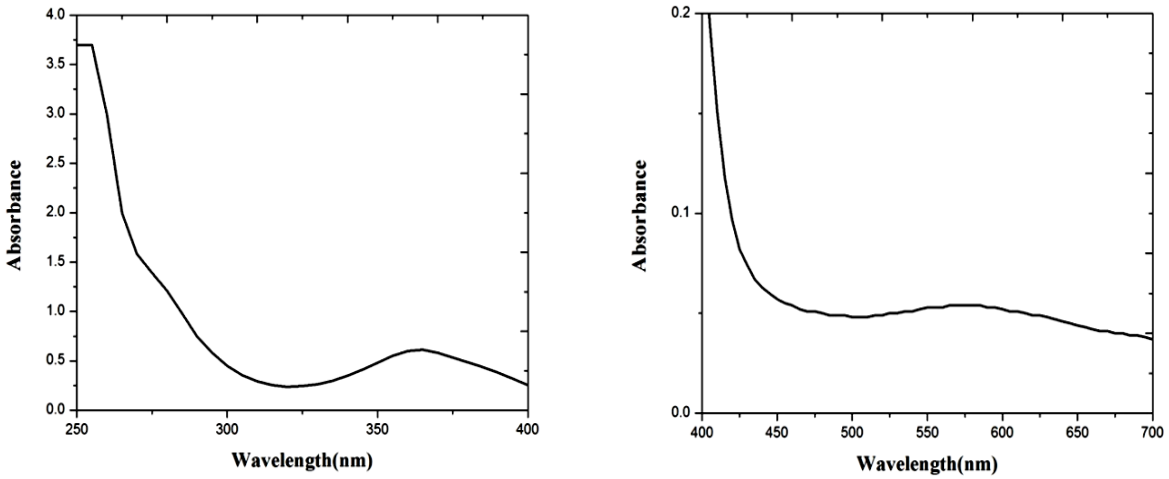

Fig. 3.9. Electronic spectrum of Cu(II) complex

3.5. 5. Thermogravimetric analysis of complexes

The thermogravimetric results of Schiff base and its metal complexes are tabulated in Table 3.4. The thermogravimetric analysis gives information about the thermal stability of the complexes and suggests a general scheme for thermal decomposition of these chelates. In the present investigation, heating rates were suitably controlled at 10^{o}C/min under nitrogen atmosphere and the weight loss was measured from the ambient temperature upto 800 ^{o}C. The thermogram of the Cr(III) complex shows two decomposition steps within the temperature range 35-300^{o}C and 300-700^{o}C which corresponds to the loss of co-ordinated water and other organic part of the ligand with a mass loss of 6.90 % (calcd: 32.02 %) and 74.57 %(calcd: 74.55 %) accompanied by two exothermic peak with t_{max}= 168.90°C and 347.90°C on the DTA curve leaving Cr_2O_3 as residue. The thermogram of the Mn(II) complex shows two decomposition steps as Cr(III) with a total mass loss of 87% leaving MnO as residue accompanied by two exothermic peak with t_{max}= 261.31°C and 305.02°C.

The thermogram of the Fe(III) and Co(II) complex shows three decomposition steps within the temperature range 35-200^{o}C, 200-500^{o}C and 500-700^{o}C with a mass loss of 6.91%(calcd: 5.98%),27.54%(calcd: 27.56%), 45.12%(calcd: 45.10%) and 2.32%(calcd: 2.35%), 27.61%(calcd: 27.58%), 61.94%(calcd: 61.96%) respectively accompanied with an exothermic peak with t_{max}=187.78°C, 309.65°C, 461.69°C and t_{max}= 129.02°C , 371.89°C , 551.00°C respectively on the DTA curve leaving Fe_2O_3 and Co_2O_3 as residue. The Ni(II) complex shows a single decomposition step between the temperature range 35-700°C having a t_{max}=350.36°C in the DTA curve which corresponds to the loss of the organic part of the ligand leaving NiO as residue. The

thermogram of the Cu(II) complex shows a loss of lattice water (t_{max}=97.85°C) in the first decomposition step (35-200°C) with a mass loss of 2.30%(cald: 2.33%) and the loss of $6NH_3$, 4CO and $C_{38}H_{24}$(t_{max}=279.35°C) in the second decomposition step (200-700°C) leaving CuO as residue[38-40]. The thermograms of all the complexes are depicted in Figs. 3.10a-f.

3. 5. 6. ESR spectral studies of copper complex

ESR studies of the Cu(II) complex are of much interest because their ground states are orbitally degenerate in regular geometries and non-degenerate in distorted geometries, since an orbitally degenerate configuration is susceptible to Jahn-Teller distortion. The interpretation of the ESR spectrum of an isolated transition metal ion yields values for two kinds of parameters.

1. Spectroscopic splitting constants (g values)
2. Hyperfine coupling constants (A values)

The ESR spectrum of Cu(II) complex (Fig.3.11) of the Schiff base ligand was recorded in the solid state at liquid nitrogen temperature. Hyperfine splitting into four lines [(I = 3/2) for Cu(II)] is seen in the low field region and four peaks in the high field region. The two major components of the g tensor in the axially symmetric field (g_{11} and $g_{\perp}$) are computed from the spectrum. The hyperfine coupling constant (A_{11}) was measured from the peaks in the low field region.g_{av} is obtained using the formula and presented in table, $\mathbf{g_{av} = 1/3g_{11}+2/3\ g_{\perp}}$

Complex	$\mathbf{g_{11}}$	$\mathbf{g_{\perp}}$	$\mathbf{g_{av}}$	$\mathbf{A_{11}}$ $\mathbf{x10^{-4}\ cm^{-1}}$	$\mathbf{g_{11}/A_{11}}$ **cm**	**G**
$[Cu(C_{17}H_{15}N_4O_2)_2].\ H_2O$	2.35	2.02	2.12	186	113	19.64

g value of the Cu(II) complex can be used to derive the ground state. In elongated octahedral and square planar complexes, the unpaired electron lies in the dx^2-y^2 orbitals giving $^2B_{1g}$ as the ground state with $g_{11} > g_{\perp}$. The low temperature EPR spectrum of the present complex is the indication of dx^2-y^2 ground state ($g_{11} > g_{\perp} > 2.03$) and thus suggest a dominally tetragonal component. The lower A_{ll} value may be due to distortion of Cu(II) geometry. This is also reflected in the value of $g_{11}/A_{11.}$ The quotient g_{11}/A_{11} is empirically treated as a measure of the distortion from planarity. The calculated value 113cm for the complex is an indication of its square planar

moderately distorted structure. In case of strong distortions, the g_{11}/A_{11} value may approach 200 cm.

G value is the most sensitive function for indicating covalency. Normally g_{11} is 2.3 or more for ionic environment and less than 2.3 for more covalent environment. For this complex, g value is less than 2.3 indicating the covalent nature of this complex which is also supported by α^2 value (0.874).

G is the axial symmetry parameter calculated using the formula,

$$\mathbf{G = g_{11}-2.0023 / g_{\perp}-2.0023}$$

If the values of G is larger than 4, the exchange interaction is negligible, while G values of less than 4 indicates considerable interaction in solid complexes. The value of exchange coupling parameter of 19.64 estimated from the spectrum suggests the absence of any exchange interaction in the complexes in the solid state. It also shows that the local tetragonal axes are only slightly misaligned and the presence of $d_{x2 - y2}$ ground state.

The MO coefficients *viz.*, in-plane σ bonding (α^2), in plane π bonding (β^2) were calculated using the formula, $\mathbf{\alpha^2 = - (A_{11}/P) + (g_{11}-2.0023) + 3/7(g_{\perp}-2.0023) + 0.04.}$ From g_{av} values, α^2 can be calculated $\mathbf{g_{av} = 2.0023-4\lambda\alpha^2 /\Delta E\ (^2_{B1g} \rightarrow {}^2_{B2g})}$. β^2 (in plane π bonding parameter) is calculated using the formula; $\mathbf{\beta^2 = (g_{11}-2.0023)\ \Delta E/-8\lambda\alpha^2}$. The value of α^2 is a measure of covaleny in in-plane σ bonding. For the present complex, it is 0.874 confirming substantial in-plane σ bonding and a appreciable degree of covalency.

Complex	α^2	β^2	K_{ll}	$K_{\perp}$
$[Cu(C_{17}H_{15}N_4O_2)_2].\ H_2O$	0.87	1.47	1.29	0.26

The values suggest the in-plane π bonding is weak. Significant information about the nature of bonding can also be derived from the magnitude of K_{11} and $K_{\perp}$. The orbital reduction factors K_{11} and $K_{\perp}$ were estimated from the expression,

$$\mathbf{K_{11} = (g_{11}-2.0023)\ \Delta E/8\lambda}$$
$$\mathbf{K_{\perp} = (g_{11}-2.0023)\ \Delta E/2\lambda}$$

λ=-828 cm^{-1}(spin – orbit coupling constant for the free ion)

In case of a pure σ bonding $K_{11} \cong K_{\perp} = 0.77$ whereas $K_{11} < K_{\perp}$ implies considerable in-plane π -bonding while for out of π- plane bonding $K_{11} > K_{\perp}$. For this complex, $K_{11} > K_{\perp}$ indicates poor in-plane π -bonding which is also reflected in β^2 values. No signals

corresponding to 1600G were observed, ruling out any Cu-Cu interaction and no dimer formation in the solid state as also verified by G values. The spin-orbit coupling constant value for the Cu ion in the complex calculated using the relation, $\mathbf{g_{av} = 2(1-2\lambda/\Delta E_{(2B1g \rightarrow 2B2g)})}$ was found to be –737.91cm^{-1} which is less than that of free Cu(II) ion =-832 cm^{-1} which also supports covalent character of M-L bond in the complex. The magnetic moment of the Cu(II) complex calculated using the formulation $\mu^2 = 3/4lgl^2$ gives μ=1.83BM which is indicative of an unpaired electron ruling out any coupling interaction between dimeric copper centers[41-44].

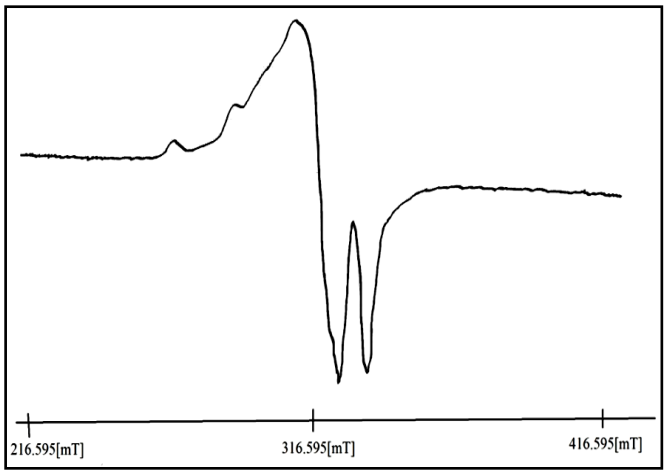

Fig. 3.11. ESR spectrum of the Cu(II) complex

3. 5. 7. Quantum chemical computational studies

3. 5. 7. 1. Theoretical structure of the ligand and Cu(II) complex

DFT study has been proven to be an important tool to obtain better insights into the geometry and electronic structure of the systems. The molecular structure of the quinoxaline schiff base ligand and Cu(II) complex was investigated theoretically. The optimized molecular structure was obtained from Gaussian 09 program (Fig. 3.12 and Fig. 3.13). Randomly selected geometric parameters (bond length and bond angles) were theortically calculated for ligand and Cu(II) complex by UB3LYP methods with basis sets listed in Table 3. 5 and 3. 6 respectively.

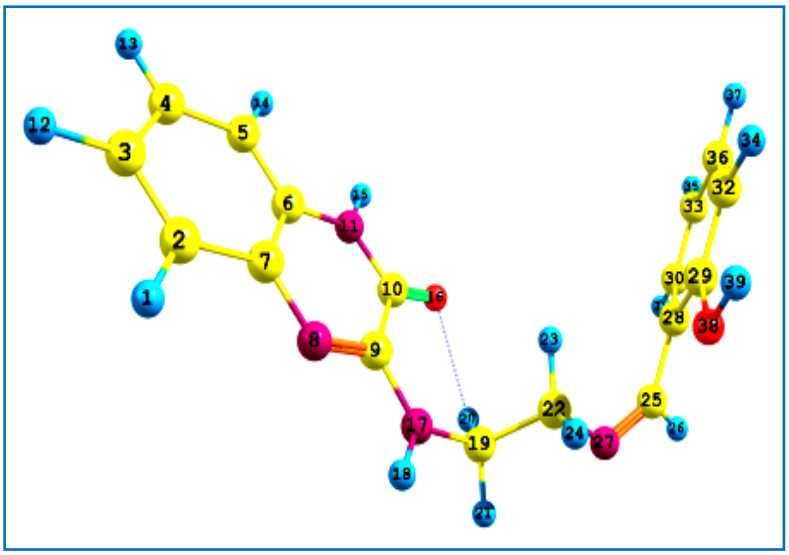

Fig. 3. 12. The optimized structure of the quinoxaline schiff base ligand

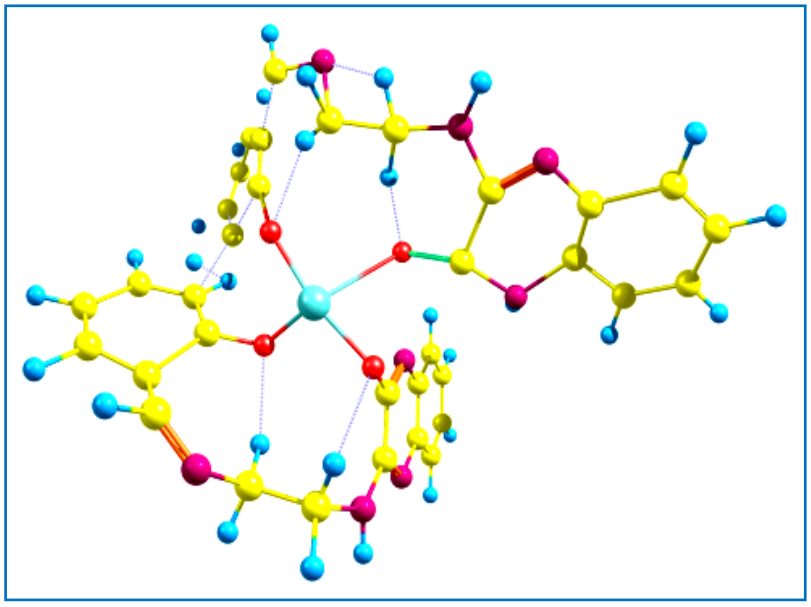

Fig. 3.13. The Optimized geometry of the Cu(II) complex

Atomic charge distributions on donor-acceptor atoms of the Cu(II) complex and donor atoms of the free ligand were calculated at B3LYP level of theory. Charge distributions between donor atom of ligands and acceptor atoms of complexes were evaluated by natural population analysis in gas phase. The charge distribution results are listed in Table 3.7. Comparing the atomic charges in Table 3.7, the atomic charge presented by the atoms O(16) and O(38) in ligand decreases after complex formation while the electron density of copper(II) cation increased. Before complexation, the charge on copper is +2, while the charge of the copper in complex is +0.79. This

indicates that ligand transfers their negative charges to copper(II) ions during formation of the complexes[45].

Table 3. 7. Atomic charges from the natural population analysis for the ligand and Cu(II) complex.

Atom	Complex	Ligand
Cu1	0.79	-
N(8)	-0.47	-0.60
N(11)	-0.42	-0.38
O(16)	-0.64	-0.52
O(38)	-0.67	-0.23
N(17)	-0.33	-0.29
N(27)	-0.70	-0.37
C(19)	-0.08	0.21
C(22)	-0.17	0.17

3. 5.7. 2. HOMO-LUMO Analysis of the ligand and the complex

The highest occupied molecular orbital (HOMO) and the lowest lying unoccupied molecular orbital (LUMO) are named as frontier molecular orbitals (FMO). The distributions and energy levels of the HOMO and LUMO orbitals computed at the UB3LYP/6-31G(d) level for the Schiff base ligand and Cu(II) complex are shown in Figs. 3.17 a and b respectively. The calculations indicate that there are 81 and 176 occupied molecular orbitals for the ligand and the Cu(II) complex respectively and the value of the energy separation between the HOMO and LUMO is -4.14 eV for the ligand, -0.00438 eV for the Cu(II) complex at the same levels respectively.

A molecule with a small frontier orbital gap is more polarisable and is generally associated with a high chemical reactivity and low kinetic stability and is also termed as soft molecule. The HOMO and LUMO energies, the energy gap(ΔE), the ionization potential(I) , the electron affinity(A), the absolute electronegativity(χ), the absolute hardness (η) and softness(S) for ligand and Cu(II) complex has been calculated at the same levels and the results are tabulated in Table 3.8.

An important topic in materials science in the past few decades has been the development of semiconductors and their broad applications in electronics and

photonics. These materials are promising in terms of their electronic properties, low cost, versatility of functionalization, thin film flexibility, ease of processing, *etc*., what is particularly exciting is the chemistry that has allowed the synthesis of molecules with narrow optical bandgaps, tunable energy levels, and desired electronic properties.

Table 3. 8. The Calculated frontier orbital energies, electronegativity, hardness and softness of ligand using UB3LYP/6-31G (d) level

	6-31G(d) Ligand	**6-31G(d) Complex**
E_{HOMO}(eV)	-5.32	-0.17
E_{LUMO}(eV)	-1.18	-0.12
I (eV)	5.32	0.17
A (eV)	1.18	0.12
χ (eV)	3.25	0.14
η (eV)	2.07	0.02
S(eV^{-1})	0.24	22.83

Such low-bandgap molecules typically having a bandgap smaller than 1.6 eV are particularly attractive in organic photovoltaics (OPV), photodetectors (PDs), and ambipolar field-effect transistors (FETs). A large number of metal complexes have been developed as phosphors for OLEDs. Better synthetic approaches and structural correlation have also been developed in recent years. Using functional group manipulation and changing metal ions, the properties of such materials have been fine-tuned. A wide color range of emitters, with high efficiencies and excellent brightness, has been achieved. Iridium and platinum complexes with quinoxaline ligands have been well established as triplet emitters. The above said Cu(II) complex with quinoxaline ligand has a very low band gap and hence can be tuned in future for photophysical properties.

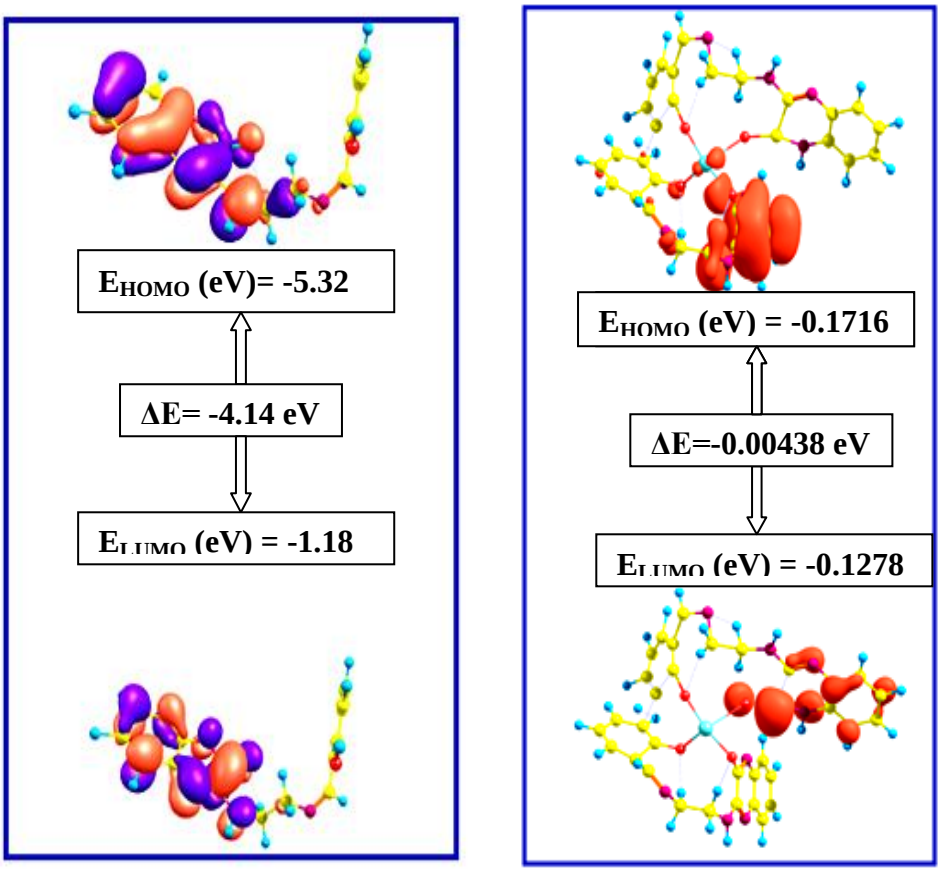

Fig. 3.14: The distribution and energy levels of the HOMO and LUMO orbitals computed at the UB3LYP/6-31G (d) level for the (a) ligand and (b) Cu(II) complex

3. 5. 8. EDAX spectral details of Cu(II) and Ni(II) complex

The chemical analysis results by EDX for the formed complexes show a homogenous distribution in between metal ions and chelating agent. The peaks of EDX profile of Cu(II) and Ni(II) complexes (Figs. 3.15a and b) refer to all elements which constitute the molecules of Schiff base complexes confirming the proposed structures. The weight percentage of the metal, carbon and nitrogen are calculated and compared with the values from analytical data and EDAX (Tables 3. 9 and 3. 10). The values are in good agreement with each other and hence the structures of the complexes are tentatively proposed as shown in Fig. 3.16.

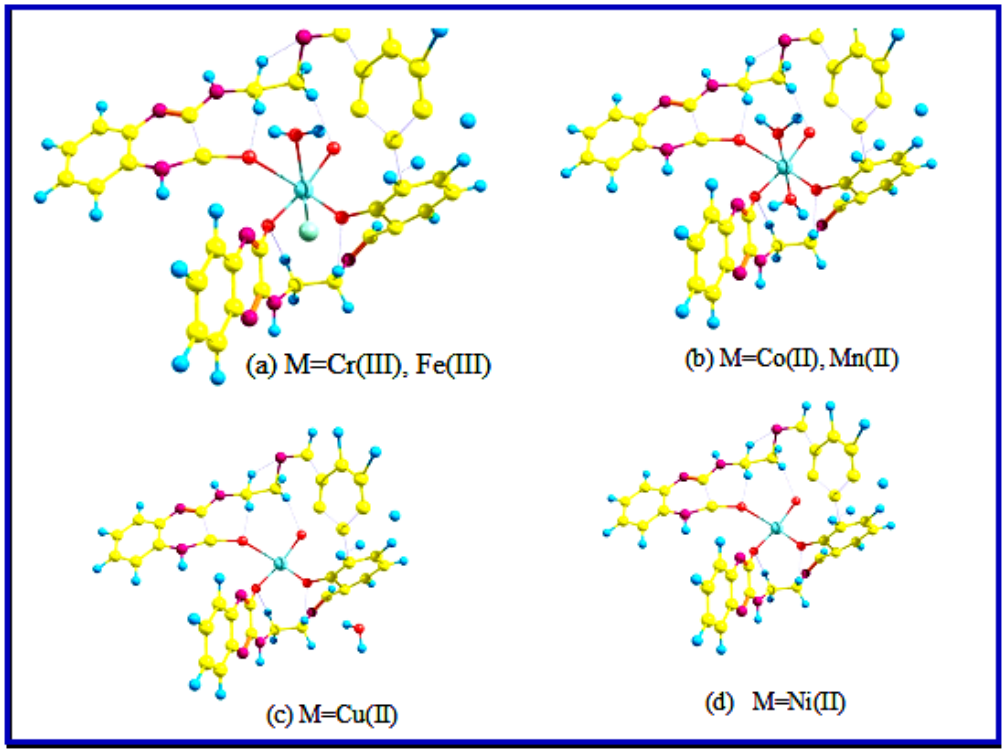

Fig. 3.16. Proposed geometry of the complexes

3. 6. Pharmacology

3. 6. 1. Antimicrobial activity

The Schiff base complexes were evaluated for their anti-proliferative and antifungal activities by inhibition zone technique against four different gram positive and gram negative bacteria *S. aureus, B. subtilis, S. paratyphi* and *K. pneumoniea* and fungi *A. niger* and *C. albicans.* The results of antibacterial and antifungal screening have been compared with the conventional standard in each case. It is evident from Tables 3. 11 and 3.12 that although the Schiff base is quite toxic, their activity increased upon complexation. The antimicrobial activity of all the complexes has been checked and found to be moderate for complexes other than Co(II) and Mn(II). The Co(II) and Mn(II) complexes showed pronounced activity against *S. aureus, S. paratyphi* and *A. niger* and considerable activity against *B. subtilis* , *K. pneumoniea* and *C. albicans* and the other complexes showed a moderate activity. It is evident from Table 3.13 that the MIC value of the Co(II) and Mn(II) complexes against *S. aureus, S. paratyphi* and *A. niger* are 250µg/ml, 125 µg/ml , 500 µg/ml and 250µg/ml, 250 µg/ml , 500 µg/ml respectively. The zone of inhibition is given in Fig. 3.17a and b for bacterial and fungal species. The increasing antimicrobial activity of the metal chelates with increase in concentration is due to the effect of metal ion on the normal

cell process. Such increased activity of the metal chelates can be explained on the basis of chelation theory. The lipid is an important factor that controls the antimicrobial activity. Tweedy's chelation theory, explains that the ion polarity of the complex is reduced by overlapping of the ligand orbitals and the exchange of the partial positive charge of the metal ion to the donor atoms of the ligand; thereby, the delocalization of p-electrons increases on the chelate ring and improves the lipophilicity of the complexes. The increment in lipophilicity increases the penetration of the complex into the lipid's membrane and blocks the metal binding sites in the microorganisms' enzymes, disturbs the process of cell respiration and the synthesis of proteins, thereby inhibiting the growth of the organism Furthermore, the mode of action of the compounds may involve formation of hydrogen bond through azomethine group with the active centers of cell constituents, resulting in interference with the normal cell process[46-49].

3. 6. 2. Anti-Cancer activity

For half a century, the field of metal based anticancer drugs has been dominated by the precious metal platinum. Cisplatin has heralded as a completely novel type of anticancer agent and its discovery enticed a veritable army of inorganic chemists to devise and test other precious metal–based therapies. The mode of action of these platinum complexes is known: the chloride or dicarboxylate ligands are hydrolysed within the cell to generate a bis-aqua species which binds irreversibly to DNA, usually to two adjacent guanine bases – and the cell unable to replicate, defaults to apoptosis (that is controlled cell death). Whilst the chemotherapeutic success of platinum is undeniable, it is by no means the perfect drug. It is not effective against many common types of cancer, drug resistance is common and it has a deplorable range of side effects, which can include nerve damage, hair loss and nausea. To overcome these limitations some compounds based on transition metals have been developed and tested against cancer cell lines. These compounds tend to cause fewer side effects compared to platinum drugs.

One of the characteristics of metals is their potential to undergo redox processes, as determined by their redox potentials. Especially, transition metal ions are usually able to switch between several oxidation states. However, not all oxidation states are observed under physiological conditions in the living organism. Due to the redox activity of metals, disturbance of the sensitive cellular redox homeostasis, a tight regulation of the metal and redox balance is crucial for health

and survival. Indeed, many of the currently used chemotherapeutic drugs have been shown to exert some interaction with the cellular redox balance and there are several attempts to specifically target the altered redox conditions in cancer cells. In contrast to most organic cancer therapeutics being redox-inactive in the cellular environment, many metal-containing drugs can undergo redox processes. These changes significantly influence and alter the physicochemical properties of such complexes including geometry, charge and reactivity. Consequently, the knowledge of the redox potential can be crucial for the understanding of the mode of action underlying the anticancer activity of metal compounds. The importance of metal based anticancer drugs increased abundantly after the success of cisplatin and its successors which are presently promising candidates in clinical evaluation. The mode of action in the anticancer drug is through the formation of metal-DNA adducts and through cellular redox homeostasis. In this case, the metal complex is more stable with Schiff base ligands and kinetically inert having a lower reactivity with biomolecules.

The synthesized complexes were checked for their cytotoxicity against human breast cancer (MCF-7) cells. Compounds were dissolved in DMSO and blank samples containing same volume of DMSO were taken as controls to identify the activity of the solvent in this cytotoxicity experiment. The results were analysed by means of cell viability curves and expressed with IC_{50} values with the studied concentration range from 0.1 to 100μM. The activity that corresponds to the inhibition of cancer cell growth at a maximum level is shown in Figs. 3.18a and 18b. The complexes showed significant IC_{50} values for the cell lines when compared to the ligand confirming that chelation of the ligands with the metal ions is responsible for the observed cytotoxic property of the complexes. Though the complexes were active against tumour cell lines under in-vitro cytotoxicity experiments none of them could attain the effectivenessof the standard drug cisplatin. The IC_{50} values of ligand, Cu(II), Ni(II), Co(II) and Mn(II) complexes are 90.13, 22.9, 54.6, 12.3 and 22.3μM respectively[50,51].

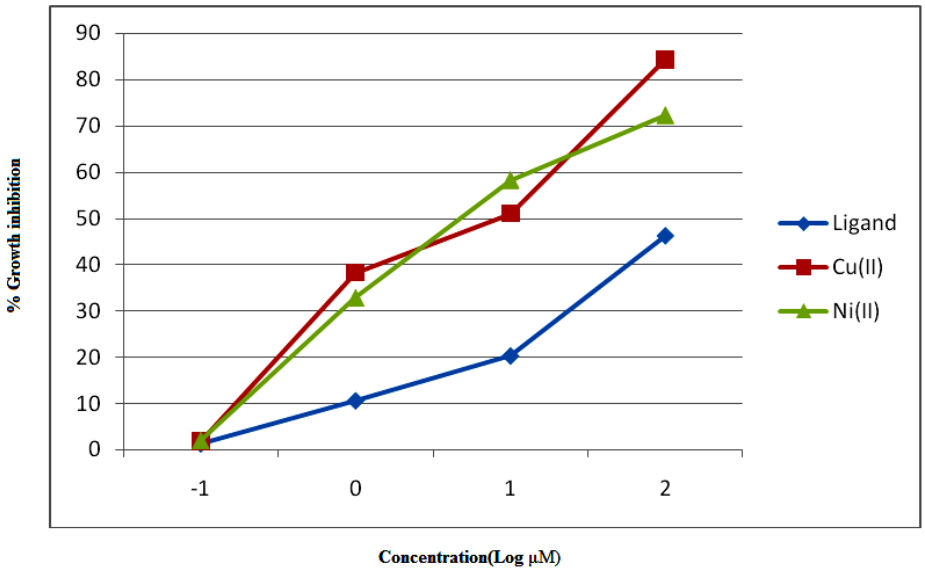

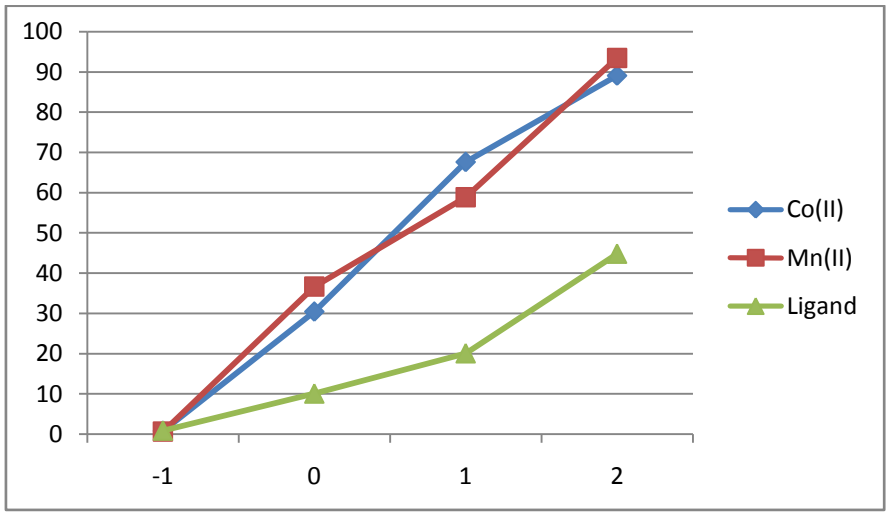

Fig. 3.18a and 18b. % Growth inhibition of MCF-7 cell line as a function of concentration of the compounds

3. 6. 3 DNA Binding

The DNA binding studies help in the analysis of non-covalent interactions of transition metal complexes with DNA which is the current area of interest in research. DNA is an important cellular receptor , many compounds exert their anticancer activity through binding to DNA , thereby changing its replications and inhibiting the growth of the tumor cells which is the basis of designing new and more efficient anticancer drugs where its effectiveness depend on the mode and affinity of the binding. So in the development of anticancer drugs, DNA binding studies play an important role and are highly significant.

Electronic absorption spectroscopy and fluorescence spectral measurements are the important tools to detect the binding modes of metal complexes with DNA.

Compounds binding through intercalation usually results in hypochromism with or without small red or blue shift, since the intercalative mode involves a strong interaction between the planar aromatic chromophores and the base pairs of DNA. The results of absorption spectra of the compounds in the absence and the presence of CT-DNA are given in Figs. 3.19a-c for Cu(II), Mn(II) and Co(II) complexes respectively. When the concentration of the DNA is increased in stepwise addition, the absorption bands of the test compounds, exhibited a hypochromism with a small blue shift. The magnitude of the intrinsic binding constants (Kb) were calculated to be 9.7×10^4 M^{-1}, 1.5×10^5 M^{-1}, 7.1×10^4 M^{-1} for Mn(II), Co(II) and Cu(II) complexes respectively. The order of binding affinity is Co(II) > Mn(II) > Cu(II). These values are less than the values of classical intercalator (*e.g.*, EB-DNA, $\approx 10^6$ M^{-1})[52-54].

The fluorescence titrations were performed to investigate the interaction mode of the complexes with DNA. The fluorescence emission intensity of the Co(II) complex is shown in Fig. 3.20, the excitation wavelength being 310 nm. The fluorescence emission intensity decreases with increasing DNA concentration and constant complex concentration. The relative binding intensity of the Co(II) complex with the CT-DNA was determined by the classical Stern-Volmer constant[55],

$$\frac{I_o}{I} = 1 + K_{sv}[Q]$$

where I_o and I represent fluorescence intensity in the absence and presence of the complex respectively. K_{sv} (L/mol) is the Stern Volmer quenching constant. However the presence of CT-DNA resulted in fluorescent quenching which might be due to the interaction of the Co(II) complex with CT-DNA. The Stern Volmer plot between Io/I and [DNA] for the quenching of the fluorescence is shown in inset graph in Fig 3.20. The binding constant values calculated from the UV-visible absorption and fluorescence spectral measurements are in accordance with each other and hence the results indicate these complexes are weak intercalators.

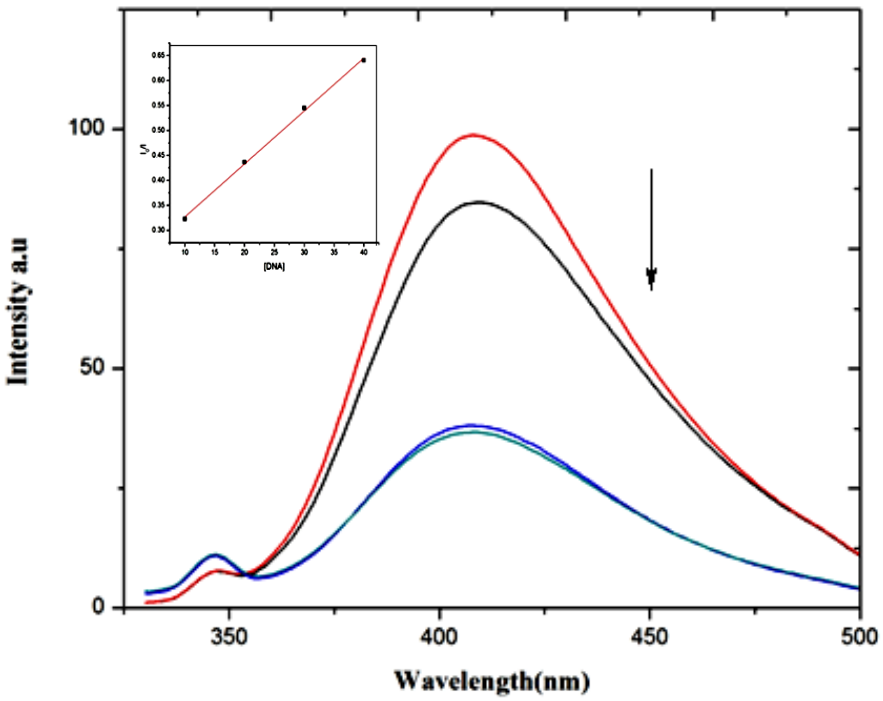

Fig. 3.20: Fluorescence emission spectrum of the Co(II) complex in the absence and presence of CT-DNA. λex = 330nm, Inset: Stern volmer plot ([DNA] vs I/Io)

3.6.4. Antioxidant activity

Since the DNA interaction experiments conducted so far revealed that the compounds exhibit good DNA binding affinity it was considered worthwhile to study the antioxidant activity of these compounds. 2, 2'-diphenyl-2-picryl-hydrazyl (DPPH) assay is widely used for assessing the ability of radical scavenging activity and it is measured in terms of IC_{50} values. Because of the presence of odd electron, DPPH shows a strong absorption band at 517 nm in the visible spectrum. As this electron becomes paired off in the presence of a free radical scavenger, this absorption vanishes and the resulting decolourisation is stoichiometric with respect to the number of electrons taken up. The DPPH assay of the tested compounds is shown in Fig. 3.21. It is seen from the results that the Mn(II) complex exhibited low activity compared to the standard ascorbic acid[56]. The order of activity of the complexes is Asc>Cu(II)>Ni(II)>Co(II)>Mn(II).

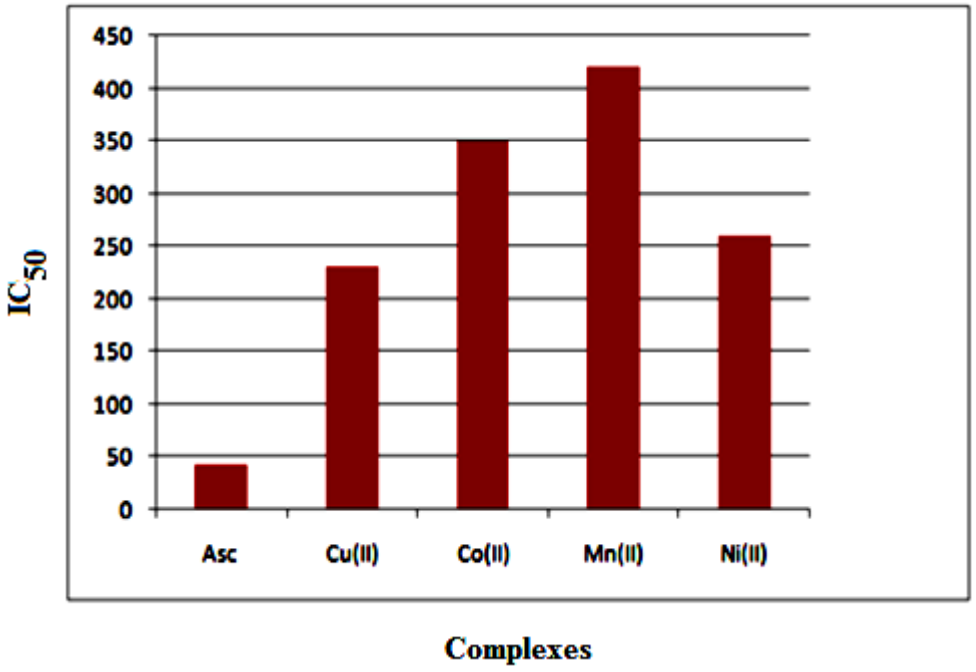

Fig. 3. 21. Antioxidant activity of the complexes with standard Ascorbic acid

3.7. Conclusion

In this study, a series of quinoxaline Schiff base complexes has been synthesized and characterized using various spectral techniques like FT-IR, electronic, TGA-DTA, NMR, ESR and EDAX. The optimized geometry of the ligand and the Cu(II) complex is optimized by UB3LYP methods with 6-31G (d) basis set. The synthesized complexes has been screened for the *in-vitro* antimicrobial activity against various test organisms and their MIC values were also reported. The complexes showed moderate to good potency against various bacterial and fungal strains developing a productive environment for the development of a new class of antimicrobial agents. The *in-vitro* anticancer activity of the ligand and the complexes were screened for all complexes and found to have good activity for the Co(II), Mn(II) and Cu(II) complexes compared with the ligand. The anti-oxidant activity of the complexes show the moderate activity for the complexes. The DNA-binding interactions of the complexes were checked and the binding constants show that Co(II) complex has a higher K_b value than the other complexes. In conclusion, the results revealed that the compounds possess significant antimicrobial and cytotoxic activity. Therefore, this study would be a fruitful matrix for the development of novel class of schiff base complexes as interesting lead molecules for further synthetic and biological evaluation.

References

1. Amin M A, Youssef M M, *Der Pharm Chemica,* **4 (**2012) 1323.
2. Chandrasekaran Y, Dutta G K, Bhaskarkanth R, Patil S, *Dyes Pigments*, **83** (2009) 162.
3. Bailly C, Echepare S, Gago F, Waring M, *Anti-Cancer Drug Des*, **15** (1999) 291.
4. Kakodar N C, Peddinti R, *Pediatr Blood Cancer*, **56** (2011) 164.
5. Lee S H, Kim N, Kim S J, Song J, Gong Y D, Kim S Y, *J Cancer Res Clin Oncol*, **139** (2013) 1279.
6. Noolvi M N, Patel H M, Bhardwaj V, Chauhan A, *Eur J Med Chem,* **46** (2011) 2327.
7. Montano D, Estela B, Caro G, Citalli L, Sanchez S, Monge M, *Bioorg Med Chem,* **21** (2013) 4550.
8. Henen M A, Serry A A, Goda F E, Nasr N A, Eisa H M, *Med Chem Res,* **21** (2012) 2368.
9. Bharagava D, Garg G, *J Pharm Res,* **5** (2012) 130.
10. Vicente E, Lima L M, Bongard E, Charnaud S, Villar R, Solano B, Burguete A, *Eur J Med Chem,* **43** (2008) 903.
11. Ganapaty S, Ramalingam P, Rao C B, *Indian J Heterocycl Chem,* **16** (2007) 283.
12. Pawar P Y, Bhise S B, *J Pharm Res,***7** (2008) 226.
13. Ahmed Khan S, Mohamed Asiri A, *Arabian J Chem,* **4** (2011) 349.
14. Elhelby A A, Awad R R, Zayed M F, *Arzneimittelforschung,* **61** (2011) 379.
15. Sridevi C H, Balaji K, Naidu A, *E-J Chem*, **7** (2010) 234.
16. Zarranz B, Jaso M, Lima L M, *Rev Bras Cienc Farm,* **42** (2006) 55.
17. Guillon J, Forfar I, Matsuda M M Desplat M and Thiolat D, *Bioorg Med Chem Lett,* **15** (2007) 191.
18. Dailey S, Feast J W, Peace R J, Sage I C, Till S,Wood E L, *J Mater Chem,* **11** (2001) 2238.
19. Asuncion B, *Bioorg Med Chem Lett*, **17** (2007) 6439.
20. Dharmchand Prasad S, Syed Riaz H, Ram Gopal, Int J Drug Dev, **2** (2010) 810.
21. Urquiola C, Vieites M, Aguirre G, *Bioorg Med Chem,* **14** (2006) 5503.
22. Xia H, Wang F, Yu K, *ActaPharmacol Sin,* **26** (2005) 1201.
23. Ghadage R V, Shirote P J, *J Chem Pharm Res*, **3** (2011) 260.
24. Anacona J R, Alvarez P, *Trans Met Chem,* **27** (2002) 856.
25. Jone Kirubavathy S, Velmurugan R, Karvembu R, Bhuvanesh N S P, Parameswari K, Chitra S, *Russ J Co-ord Chem,* **41** (2015) 345.

26. Xing T, Zhan S, Li Y, Wu Z,Yan C, *J Co-ord Chem*, (2013) 3149.
27. Zhang S, Chun X, Chen Y, Zhou J, *Chin J Chem*, **29** (2011) 65.
28. Prabhakaran R, Anantharaman S, Thilagavathi M, Kaveri M V, Kalaivani P, Karvembu R, Dharmaraj N , Bertagnolli H , Daller-mer F, Natarajan K, *Spectrochim Acta A Mol Biomol Spectrosc.* **78** (2011) 844.
29. Abd El-Halim H F, Omar M M , Mohamed G G, El-elasayed M A, *Eur J Chem,* **2** (2011) 178.
30. Ananthalakshmi P V, Sandhyarani D, Jayatyagaraju V, *Asian J Chem,* **7** (1995) 296.
31. Al-Nahary T T, *J Saudi Chem Soc,* **13** (2009) 253.
32. Alhadi A A, Shaker S A, Yehye W A, Ali H M and Abdullah M A, *Bull Chem Soc Ehiop,* **26** (2012) 95.
33. Patil R M, Prabhu M M, *Int J Chem Sci,* **8** (2010) 52.
34. Dubey R K, Dubey U K, Mishra C M, *Indain J Chem,* **45A** (2006) 1638.
35. Raman N, Pichaikani Raja, Kulandisamy A, *Proc Indian Acad Sci(Chem Sci),* **113** (2001) 183.
36. Munde A S, Shelke V A , Jadhav S M, Kirdant A S, Vaidhya S R, Shankarwar S G, Chondhekar T K , *Adv Appl Sci Res,* **3** (2012) 175.
37. Gudari K B, Patil S A, Ramesh S, Shenoy V, Patil M S, *J Serb Chem Soc,* **71** (2006) 529.
38. Munde A S, Jagdale A N, Jadhav S M, Chondhekar T K, *J Serb Chem Soc,* **75** (2010) 349.
39. Khedr A M, Marwani H M, *Int J Electrochem Sci,* **7** (2012) 10074.
40. Tas E, Kilic A, Durgun M, Kupecik L, Yilmez I, Arslan S, *Spectrochim Acta A Mol Biomol Spectrosc*, **75** (2010) 811.
41. El-Tabl A S, *Trans Met Chem,* **23** (1998) 63.
42. Raman N , Ravichandran S, Thangaraja C , *J Chem Sci,* **116** (2004) 215.
43. Raman N, Dhaveethu Raja J, *Indian J Chem,* **46A** (2007) 1611.
44. Anupama B, Venkataramanareddy C H, Gyanakumari C, *Chem Sci Trans,* **2** (2013) 461.
45. Duran K, Koray S, *Indian J Chem,* **52A** (2013) 480.
46. Tharmaraj P, Kodimunthiri D, Sheela C D, Shanmugapriya C S, *J Serb Chem Soc,* **74** (2009) 927.

47. Pelczar, M J , Chan E C S , Krieg N R 1996 *Microbiology*, McGraw-Hill, New York, USA.
48. Mane P S, Shirodkar S G, Arbad B R, Chondhekar T K, *Indian J Chem,* **40A** (2001) 648.
49. Mishra L , Singh V K, *Indian J Chem,* **32A** (1993) 446.
50. Dharmaraj N, Vishwanathamurthi P, Natarajan K, *Trans Met Chem*, **26** (2001) 105.
51. Umesha K B, Rai K M L, Harish Nayaka M A, *Int J Biomed Sci,* **5** (2009) 359.
52. Rekha H S, Basavaraj P R, Dayanandha B S, Chandrashekhar V M, Muchchandi I S, Kalagonda G B, *Appl Organomet. Chem,* **29** (2015) 101.
53. Kurdekar G S, Puttanagouda S M, Kulkarni N V, Budagumpi S, Revankar V K, *Med Chem Res*, **20** (2011) 421.
54. Chandrasekaran S, Sameena Y, MuthuVijayan Enoch I V, *Turk J Chem*, **38** (2014) 725.
55. Chandrasekaran S, Sameena Y, MuthuVijayan Enoch I V, *Australian J Chem,* **67** (2013) 256.
56. Sampath K, Sathiyaraj S, Jayabalakrishnan C, *Spectrochim Acta A Mol Biomol Spectrosc*, **115** (2013) 287.